Quantitative analysis of nanoscale electronic properties in an $Al_xGa_{1-x}N$/GaN heterostructure field-effect transistor structure

D. M. Schaadt, E. J. Miller, and E. T. Yu[a)]
Department of Electrical and Computer Engineering, University of California, San Diego, La Jolla, California 92093-0407

J. M. Redwing
ATMI/Epitronics, 21002 North 19th Avenue, Suite 5, Phoenix, Arizona 85027-2726

(Received 7 January 2001; accepted 21 May 2001)

Local dC/dV spectroscopy performed in a scanning capacitance microscope is used to map, quantitatively and with high spatial resolution, lateral variations in the threshold voltage of an $Al_xGa_{1-x}N$/GaN heterostructure field-effect transistor epitaxial layer structure. Theoretical analysis and numerical simulations are used to quantify charge concentrations, the corresponding threshold voltage shifts, and the influence of the measurement apparatus on these results. High-resolution scanning capacitance and the associated threshold voltage images reveal round features <150 nm in diameter within which a shift in threshold voltage of about 1.5–2 V is measured. Theoretical analysis and numerical simulations indicate that these features are consistent with the presence of charged threading dislocations with a linear charge density of $\sim 10^7$ e/cm^{-1} that cause localized partial or full depletion of carriers from the two-dimensional electron gas. Large-scale scanning capacitance images reveal variations in contrast over areas several microns in size with corresponding threshold voltage shifts of approximately 1 V. These large features are postulated to arise from a combination of thickness and composition variations in the $Al_xGa_{1-x}N$ layer. © *2001 American Vacuum Society.* [DOI: 10.1116/1.1385914]

I. INTRODUCTION

$Al_xGa_{1-x}N$/GaN heterostructure field-effect transistors (HFETs) have attracted intense research interest due to their importance for microwave and high-temperature/high-power electronic applications.[1–6] However, high threading dislocation densities ($\sim 10^8-10^{10}$ cm^{-2}), which are a result of the significant lattice mismatch between GaN and commonly used substrates such as sapphire or SiC, are typically present and can lead to increased carrier scattering[7] and high concentrations of acceptor-like trap levels.[8] It has been observed that potential shifts of up to 1.5 V may be present near a dislocation in *n*-type GaN;[9] in an $Al_xGa_{1-x}N$/GaN HFET epitaxial layer structure, defects such as dislocations as well as the presence of thickness and composition variations in the $Al_xGa_{1-x}N$ layer can result in pronounced variations in the local HFET threshold voltage V_T.[10,11] We have recently used spatially resolved scanning capacitance microscopy to obtain quantitative experimental information and to directly correlate shifts in threshold voltage in an $Al_xGa_{1-x}N$/GaN HFET with the presence of threading dislocations, thickness and composition variations, and other defects.[12] The observed shifts in V_T and their spatial distribution were consistent with the presence of charged threading dislocations in the epitaxial layer structure and with localized thickness and composition variations in the $Al_xGa_{1-x}N$ layer.

In this article, we present a detailed description of the measurement technique, compare the analytical model from Ref. 12 with simulations of electrostatic potential and electron concentration near a threading dislocation, and analyze the influence of the scanning capacitance microscope (SCM) probe tip on the measured signal, image contrast, and quantification of HFET threshold voltage variations.

II. EXPERIMENT

All measurements were performed with a grounded, heavily p^+-doped Si probe tip in a Digital Instruments 3100 SCM under ambient conditions with a bias applied to Ti/Al ohmic contacts fabricated on the sample, as shown in Fig. 1. The sample used in these studies consisted of a 23 nm undoped $Al_{0.26}Ga_{0.74}N$/1.2 μm undoped GaN/0.1 μm AlN heterostructure grown on 4*H*-SiC (0001) by metal organic chemical vapor deposition. Ohmic contacts were made to the sample by the evaporation of 33 nm Ti/77 nm Al and subsequent annealing at 750 °C for 1.5 min. Due to the polarization field in the strained $Al_xGa_{1-x}N$ layer, a two-dimensional electron gas (2DEG) is created at zero bias at the $Al_xGa_{1-x}N$/GaN interface, even in absence of intentional doping.[13–15]

To obtain a threshold voltage map, we reduced the scan area to 1 nm$\times$1 nm for high-resolution, small-area scans and to 500 nm$\times$500 nm for lower-resolution, large-area scans, thus effectively averaging the data over these areas. dC/dV spectra were obtained as functions of tip–sample bias, with the applied voltage signal consisting of the internal SCM high-frequency ac bias (with an amplitude of 2 V at 100 kHz) plus an externally applied triangle–wave bias signal, which was ramped from 0 to 8 V at a frequency of 5 Hz. To reduce noise, we recorded and averaged multiple (typically 50 to 400) dC/dV versus V curves. We then moved the tip to successive positions in steps of 50 nm for small area scans and in steps of 1 μm for large-area scans and repeated the procedure. The dC/dV versus V data were processed by sub-

a)Electronic mail: ety@ece.ucsd.edu

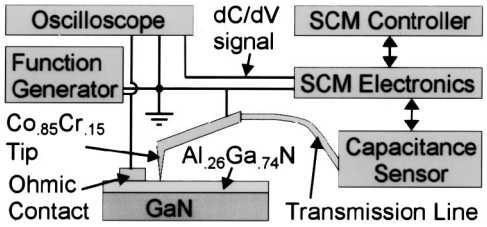

FIG. 1. Experimental configuration for local dC/dV spectroscopy in a SCM is shown.

tracting a line fitted to a background that arises from uncompensated stray capacitances, and then normalizing to a peak height of unity.

III. RESULTS AND DISCUSSION

We previously presented topography images, scanning capacitance images, and the associated threshold voltage maps derived from high-resolution (950 nm×700 nm) and large-area (40 μm×15 μm) scan areas of an $Al_xGa_{1-x}N$/GaN HFET epitaxial layer structure.[12] Small round features with a radius of about 50–70 nm were observed in the 950 nm ×700 nm SCM scan, while the large-area scan showed features, typically several microns in size, which were similar, but did not directly correlate, to the structure observed in the topography image. Threshold voltage maps were obtained by integrating dC/dV data twice and subsequent linear extrapolation of the charge within the 2DEG, and showed features corresponding to those in the SCM images.

The small round features in the smaller scan were found, on the basis of a simple analytical treatment, to be consistent with the presence of charged threading dislocations at a density of about 10^9 cm^{-2} in the sample. Several groups have reported that threading dislocations in III–V nitride heterostructures can produce acceptor-like trap states[8] which become negatively charged.[16,17] This charge can result in the depletion of the 2DEG at the $Al_xGa_{1-x}N$/GaN interface,[11] causing a shift in threshold voltage near the threading dislocations which would be observed in the scanning capacitance data and the V_T map.

We have estimated analytically the effect of a charged threading dislocation on the contrast feature observed in a scanning capacitance image as well as on the local shift in threshold voltage.[12] This estimate is then compared with results of detailed numerical simulations of the $Al_xGa_{1-x}N$/GaN sample structure and the SCM probe tip. Assuming a tip with a radius of curvature of about 15 nm, we obtained an actual feature radius of about 35–60 nm for an observed feature radius of about 50–75 nm due solely to the convolution of the actual feature with the tip shape, as typically occurs in scanning probe measurements. In addition, the observed feature radius is further increased due to the presence of a depletion region approximately 30 nm in size, induced by the probe tip, in the $Al_xGa_{1-x}N$ layer. This resulted in a final actual feature radius of about 30 nm or smaller.

A charged threading dislocation line is modeled simply as a continuous line charge, the potential due to which, assuming cylindrical symmetry and screening by ionized impurities and free electrons, is given by[18]

$$U(r)=\frac{1}{4\pi\epsilon\epsilon_0}2q\gamma K_0\left(\frac{r}{\lambda_D}\right), \tag{1}$$

where λ_D is the Debye length, given by

$$\lambda_D=\sqrt{\frac{kT\epsilon\epsilon_0}{q^2N_d}}. \tag{2}$$

In Eqs. (1) and (2), ϵ is the relative dielectric constant, ϵ_0 the vacuum permittivity, q the electron charge, γ the line charge density, K_0 the modified Bessel function of the second kind of zeroth order, r the distance from the line, k the Boltzmann constant, T the temperature, and N_d the background dopant density. We can use Eq. (1) to describe the potential due to a charged threading dislocation by setting the line charge density to $\gamma=f/c$, where f is the fraction of filled traps (ranging from 0 to 1) and c the [0001] lattice constant of $Al_xGa_{1-x}N$. Assuming a dislocation density of roughly 10^9 cm^{-2} and a background dopant density of about 10^{18} cm^{-3} within the $Al_xGa_{1-x}N$ layer, one obtains[19] $f\approx 0.5$ and a Debye length of about 3.5 nm at 300 K. The effect of the potential $U(r)$ ceases to be significant when $U(r)\lesssim kT$, i.e., when $r\gtrsim 3.25\,\lambda_D$. On this basis, we obtain an estimated feature radius of about 11 nm, which is well within the above mentioned range of 30 nm or smaller.

In the vicinity of these features, the maximum threshold voltage shift ΔV_T from the average value was about 1.5–2 V, which is consistent with previous measurements by Hansen *et al.*[9] Using the expression $Q=-C\Delta V_T$, where C is the capacitance per unit area of the $Al_xGa_{1-x}N$ barrier layer, we estimate the measured ΔV_T to correspond to a charge Q of about -3.4×10^{12} e/cm^2 to -4.6×10^{12} e/cm^2. This value is approximately equal to the amount of charge expected to be contained, within the $Al_xGa_{1-x}N$ barrier layer and an area equal to the tip size, on a threading dislocation with linear charge density of about $-10^7\approx-0.5$ e/cm.

To more accurately estimate the effect of the tip size on the potential, we have modeled and numerically simulated the electrostatic potential distribution and electron concentration for the device structure shown in Fig. 2(a). The tip is modeled as a box consisting of Co with a 10 nm×10 nm contact area to the $Al_xGa_{1-x}N$ layer. The polarization charge is represented using ionized dopants at the $Al_xGa_{1-x}N$/GaN interface. To simulate the charged threading dislocation, ionized dopants are placed in a rectangular column with a 1 nm×1 nm base, extending through the $Al_xGa_{1-x}N$ and GaN layers at the center of the tip area. The dopant concentration is chosen to match the aforementioned linear charge density of -10^7 e/cm.

The relative potential ϕ_{rel}, i.e., the change in potential between simulations with and without the charged threading dislocation, at a zero tip bias and as a function of distance from the tip center, is shown in the top part of Fig. 2(b) as a solid line. For comparison, the relative potential due to the charged threading dislocation derived analytically and given

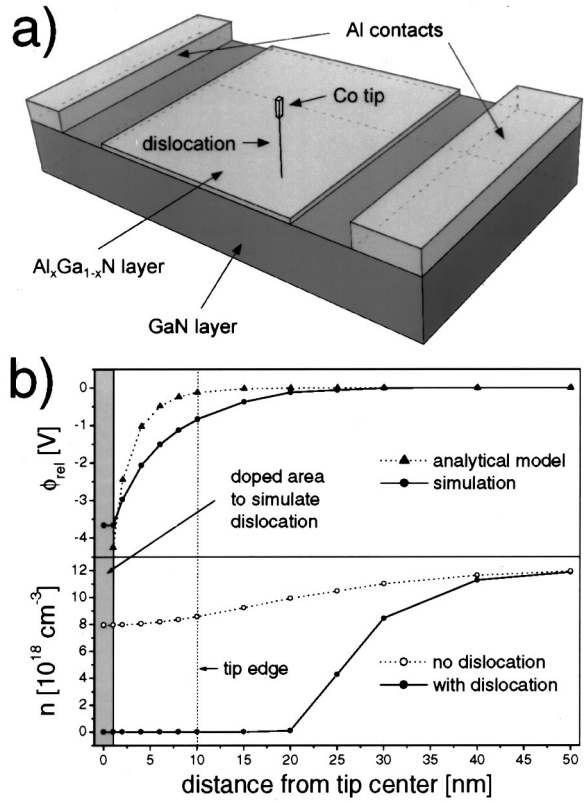

FIG. 2. (a) Schematic diagram of the simulated structure with a dislocation line placed at the center of the tip area and extending through the $Al_xGa_{1-x}N$ and GaN layers is shown. (b) Top: plots of the potential variation due to a charged threading dislocation calculated analytically (solid line) and via simulation (dotted line) and bottom: electron concentration at the $Al_xGa_{1-x}N$/GaN interface as a function of distance from the tip center are shown.

by Eq. (1) is plotted in the top part of Fig. 2(b) as a dotted line. The simulated relative potential becomes equal to kT at a distance of approximately 25 nm from the tip center or, equivalently, from the dislocation core. The simulated relative potential is in fairly good qualitative agreement with the potential from Eq. (1). The difference in the potentials in the immediate vicinity of the dislocation core is a result of the potential due to the tip. This effect is also visible in the plot of the electron concentration at the $Al_xGa_{1-x}N$/GaN interface, i.e., the electron concentration in the 2DEG, for the simulation conducted without the charged threading dislocation present, shown in the bottom part of Fig. 2(b) as dotted line, where the potential due to the tip results in a small reduction of the electron concentration.

The electron concentration at the $Al_xGa_{1-x}N$/GaN interface for a simulation performed in the vicinity of a charged threading dislocation line is shown as a solid line in the bottom part of Fig. 2(b). The effect of the charge present on the threading dislocation can be seen most clearly in the partial to full depletion of the 2DEG charge up to about 25 nm distant from the dislocation core. Due to the effect of the tip size, the depletion region obtained in the simulation is somewhat larger than the value obtained from the analytical model, but in very good agreement with the aforementioned actual feature radius, estimated to be about 30 nm or smaller.

We can derive values for the shift in threshold voltage in the vicinity of a charged threading dislocation using simulations with and without a dislocation present in a similar manner to that described in Ref. 12. Specifically, linear extrapolation of a plot of integrated charge density within the depletion region (i.e., from 0 to 25 nm) versus the applied tip bias to a zero charge concentration is used to define the threshold voltage. We then obtain values for V_T of -3.46 V for a simulation without a dislocation present, and -2.11 V for a simulation with the tip placed directly atop a charged threading dislocation. The resulting shift in threshold voltage $\Delta V_T \approx 1.35$ V is in excellent accord with the experimentally measured values of 1.5–2 V. Thus, our results confirm that the simple analytical model and detailed numerical simulations yield consistent results, with the simulations being more precise with respect to the effect of the tip size on the potential and electron concentration.

Large-area scans ($40\,\mu m \times 15\,\mu m$) scans revealed the presence of substantial threshold voltage shifts, as large as ± 1 V or more, relative to the average threshold voltage value of -4.8 V over length scales of approximately one to several μm. These features were comparable in size to features observed in atomic force microscopy topographic images, suggesting that thickness variations in the $Al_xGa_{1-x}N$ layer might play a substantial role in the measured V_T variations, as postulated on the basis of previously reported SCM studies.[10,11] Using a theoretical expression for the sheet carrier concentration, we estimated the threshold voltage shift due to a change in thickness in the $Al_xGa_{1-x}N$ layer. For an Al concentration of 26% and a layer thickness $d = 23$ nm, we obtain an approximate polarization sheet charge density of 1.25×10^{13} e/cm^2,[20] which results in a threshold voltage shift of about 0.25 V for a thickness change of about 1 nm, i.e., approximately 5%. Using a similar approach, we calculated that a composition variation of about 5% in the $Al_xGa_{1-x}N$ layer would yield a change in threshold voltage comparable to that of a 1 nm thickness variation. The observed larger variations in ΔV_T of more than 1 V might therefore be a consequence of a combination of thickness and composition variations in the $Al_xGa_{1-x}N$ layer.

To further distinguish between the thickness and composition variations, both of which can give rise to substantial local variations in V_T, we can analyze the dC/dV signal and the peak size in the dC/dV versus V data, as shown in Fig. 3(a). Ideally, one might expect that the thickness variations within the $Al_xGa_{1-x}N$ layer could be extracted from the capacitance $C \approx \epsilon\epsilon_0 A/d$, where A is the effective tip area and d is the local $Al_xGa_{1-x}N$ layer thickness, and that this capacitance could be obtained from an integration of the dC/dV signal. However, the integrated capacitance depends on the peak width, which is not constant over the measurement area as shown in Fig. 3(c). Thus, the attempted extraction of thickness variations directly from the integrated capacitance could lead to artifacts.

However, since the dC/dV peak height is also proportional to the capacitance of the $Al_xGa_{1-x}N$ layer, we can

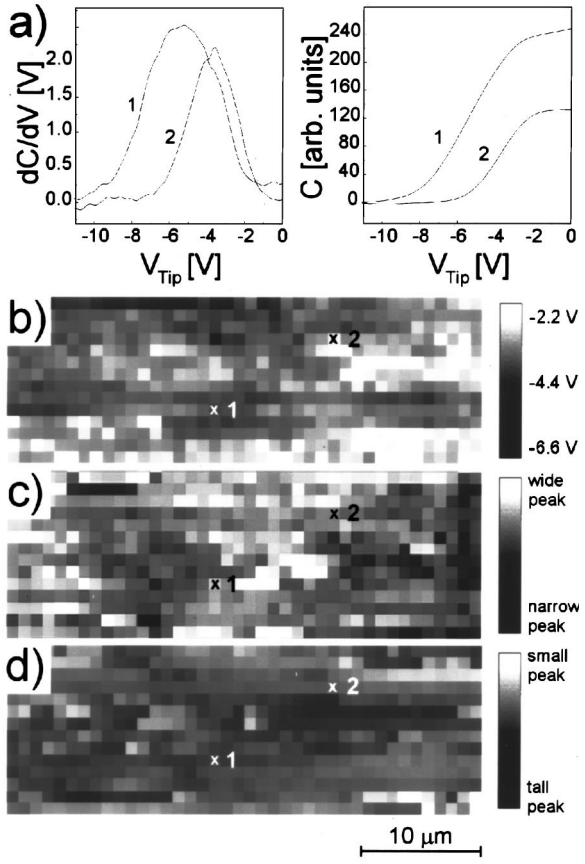

FIG. 3. (a) SCM signal (left-hand side plot) and integrated capacitance–voltage spectra (right-hand side plot) corresponding to locations indicated in the images are shown. (b) 40 μm$\times$15 μm threshold voltage image is presented. (c) Map of dC/dV signal peak width for the same scan area as in (b); the peak width varies over the measurement area and thus influences the integrated capacitance. (d) Map of dC/dV signal peak height for the same scan area as in (b); the peak height map is only partially correlated with the threshold voltage map, indicating that threshold voltage variations arise from variations in both $Al_xGa_{1-x}N$ thickness and composition.

obtain thickness information from a plot of the peak height, as shown in Fig. 3(d). Bright areas in this image correspond to large-amplitude peaks, i.e., a thin $Al_xGa_{1-x}N$ layer, while dark areas correspond to small peaks, i.e., a thick $Al_xGa_{1-x}N$ layer. A thick layer would result in a more negative threshold voltage, which would correspond to a dark area in the threshold voltage map in Fig. 3(b). If the variations in threshold voltage would be caused purely by thickness variations, the threshold voltage map and the map of the peak height should be very closely correlated across the entire image area, which is not the case. Thus, the variations in threshold voltage are probably due to a combination of thickness and compositional variations.

IV. CONCLUSIONS

In conclusion, we have used local dC/dV spectroscopy performed in a SCM to quantify and map the threshold voltage distribution in an $Al_xGa_{1-x}N$/GaN HFET structure. Small round features, which exhibited a threshold voltage shift of about 1.5–2 V compared to the average threshold voltage, were attributed to the effect of the electrostatic potential of charged threading dislocations that cause localized reduction or depletion of carriers from the 2DEG. An analytical model and simulations of electrostatic potential and electron concentration were compared and used to explain the observed features. The results obtained with the analytical model and the simulations were in good agreement, with the simulation allowing a somewhat more accurate quantitative description of the effect of the tip size on the electrostatic potential and the electron concentration. Larger features, several μm in size with corresponding threshold voltage shifts of up to 1 V or more, were observed in large-area scans. A detailed analysis of the SCM signal showed that these features are not purely a result of thickness variations in the $Al_xGa_{1-x}N$ layer, but are most likely attributable to a combination of thickness and composition variations.

ACKNOWLEDGMENTS

The authors thank Dr. X. Z. Dang for help in the fabrication of the ohmic contacts. Part of this work was supported by ONR under Grant Nos. N00014-99-1-0729 (POLARIS MURI, Dr. Colin Wood) and N00014-99-1-0545 (DURIP, Dr. John Zolper) and by BMDO (Dr. Kepi Wu).

[1]O. Aktas, Z. F. Fan, A. Botchkarev, S. N. Mohammad, M. Roth, T. Jenkins, L. Kehias, and H. Morkoc, IEEE Electron Device Lett. **18**, 293 (1997).
[2]M. A. Khan, Q. Chen, M. S. Shur, B. T. Dermott, J. A. Higgins, J. Burm, W. J. Schaff, and L. F. Eastman, Solid-State Electron. **41**, 1555 (1997).
[3]G. J. Sullivan, M. Y. Chen, J. A. Higgins, J. W. Yang, Q. Chen, R. L. Pierson, and B. T. McDermott, IEEE Electron Device Lett. **19**, 198 (1998).
[4]Y. F. Wu, B. P. Keller, S. Keller, J. J. Xu, B. J. Thibeault, S. P. Denbaars, and U. K. Mishra, IEICE Trans. Electron. **E82-C**, 1895 (1999).
[5]S. T. Sheppard, K. Doverspike, W. L. Pribble, S. T. Allen, J. W. Palmour, L. T. Kehias, and T. J. Jenkins, IEEE Electron Device Lett. **20**, 161 (1999).
[6]N. X. Nguyen, M. Micovic, W. S. Wong, P. Hashimoto, L. M. McCray, P. Janke, and C. Nguyen, Electron. Lett. **36**, 468 (2000).
[7]H. M. Ng, D. Doppalapudi, T. D. Moustakas, N. G. Weimann, and L. F. Eastman, Appl. Phys. Lett. **73**, 821 (1998).
[8]F. A. Ponce, D. P. Bour, W. Götz, and P. J. Wright, Appl. Phys. Lett. **68**, 57 (1996).
[9]P. J. Hansen, Y. E. Strausser, A. N. Erickson, E. J. Tarsa, P. Kozodoy, E. G. Brazel, J. P. Ibbetson, U. Mishra, V. Narayanamurti, S. P. DenBaars, and J. S. Speck, Appl. Phys. Lett. **72**, 2247 (1998).
[10]K. V. Smith, E. T. Yu, J. M. Redwing, and K. S. Boutros, Appl. Phys. Lett. **75**, 2250 (1999).
[11]K. V. Smith, E. T. Yu, J. M. Redwing, and K. S. Boutros, J. Electron. Mater. **29**, 274 (2000).
[12]D. M. Schaadt, E. J. Miller, E. T. Yu, and J. M. Redwing, Appl. Phys. Lett. **78**, 88 (2001).
[13]A. Bykhovski, B. Gelmont, and M. Shur, J. Appl. Phys. **74**, 6734 (1993).
[14]P. M. Asbeck, E. T. Yu, S. S. Lau, G. J. Sullivan, J. Van Hove, and J. M. Redwing, Electron. Lett. **33**, 1230 (1997).
[15]E. T. Yu, G. J. Sullivan, P. M. Asbeck, C. D. Wang, D. Qiao, and S. S. Lau, Appl. Phys. Lett. **71**, 2794 (1997).
[16]K. Leung, A. F. Wright, and E. B. Stechel, Appl. Phys. Lett. **74**, 2495 (1999).
[17]M. Haugk, J. Elsner, T. Frauenheim, T. E. M. Staab, C. D. Latham, R. Jones, H. S. Leipner, T. Heine, G. Seifert, and M. Sternberg, Phys. Status Solidi B **217**, 473 (2000).
[18]B. Pödör, Phys. Status Solidi **16**, K167 (1966).
[19]N. G. Weinmann, L. F. Eastman, D. Doppalapudi, H. M. Ng, and T. D. Moustakas, J. Appl. Phys. **83**, 3656 (1998).
[20]E. T. Yu, *III–V Nitride Semiconductors: Applications and Devices*, edited by E. T. Yu and O. Manasreh (Gordon and Breach, New York, 2000).